ALTERNATIVE OPTICS DESIGN OF THE CLIC DAMPING RINGS WITH VARIABLE DIPOLE BENDS AND HIGH-FIELD WIGGLERS

S. Papadopoulou, F. Antoniou, Y. Papaphilippou, CERN, Geneva, Switzerland

Abstract

The CLIC Damping Rings baseline design aims to reach an ultra-low horizontal normalised emittance of 500 nm-rad at 2.86 GeV, based on the combined effect of TME arc cells and high-field super-conducting damping wigglers, while keeping the ring as compact as possible. In this paper, an alternative design is described, based on TME cells with longitudinally variable bends and an optimized Nb_3Sn high-field wiggler. The impact of these changes on ring optics parameters and the associated optimisation steps are detailed taking into account the dominant effect of intrabeam scattering.

LAYOUT AND DESIGN REQUIREMENTS

The CLIC Damping rings (DRs) have to accommodate a 2.86 GeV beam and should damp it down to normalized horizontal and vertical emittances of 500 nm-rad and 5 nm-rad respectively. The longitudinal normalised emittance should be kept below 6 keV·m. The requirements for ultra-low emittances in all three planes give rise to a series of collective effects [1], with intrabeam scattering (IBS) being the dominant one.

The DRs' layout consists of a racetrack with two arcs and two long straight sections (LSS). The arcs are composed by theoretical minimum emittance (TME) cells and the LSS by FODO cells filled with damping wigglers. Space is also reserved for RF cavities, injection and extraction equipment [2]. The lattice functions between the arcs and the straight sections are matched from the dispersion suppressors and beta matching sections.

In this paper, an alternative design using longitudinally variable bends in the arc TME cells and an optimized high-field wiggler in the FODO cells is proposed. Through this approach, it is possible to achieve the desired output parameters and at the same time decrease the ring's circumference.

LONGITUDINALLY VARIABLE BENDS

Longitudinally variable dipoles, whose magnetic field varies along their length, can provide lower horizontal emittances than a uniform dipole of the same bending angle [3,4]. Actually in order to achieve that, the bending radius ρ_x of a variable bend should have an evolution similar to the one of the uniform dipole's dispersion invariant $\mathcal{H}(s)$ [5–9]: maximum magnetic field should be applied at their center, and it should be decreasing towards the edge of the dipole.

Two examples of variable bends are presented in this paper, they are described by the bending radii forming a step (green line) and a trapezium shape (blue line), as shown in Fig. 1. They are characterised by two lengths L_1 and L_2 with different bending radii ρ_1 and ρ_2. The evolution of the
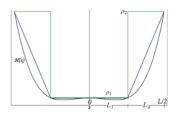

Figure 1: The evolution of the dispersion invariant $\mathcal{H}(s)$ along the uniform dipole (black line) and the bending radius evolution along the variable bends- coloured with green for the step and with blue for the trapezium profile.

bending radius ρ_{st} and ρ_{tr}, for the step and the trapezium profile, respectively, are:

$$\rho_{st}(s)= \begin{cases} \rho_1, & 0 < s < L_1 \\ \rho_2, & L_1 < s < L_1 + L_2 \end{cases}$$

$$\rho_{tr}(s)= \begin{cases} \rho_1, & 0 < s < L_1 \\ \rho_1 + \dfrac{(L_1 - s)(\rho_1 - \rho_2)}{L_2}, & L_1 < s < L_1 + L_2 \end{cases}$$

The emittance reduction factor $F_{TME} = \epsilon_{TME_{uni}}/\epsilon_{TME_{var}}$ is the ratio of the absolute minimum emittances of a uniform with respect to a variable field dipole, and its parametric behaviour can be obtained using analytical expressions for the TME cells [9]. For this study, it is useful to define the lengths and bending radii ratios as $\lambda = L_1/L_2$ and $\rho = \rho_1/\rho_2$, respectively. In Fig. 2, the F_{TME} is parametrized with ρ and λ with the restriction of $\lambda > 0.1$, for the step (left) and the trapezium (right) profile. The areas where F_{TME} is high are blue-colored, while red-colored are the
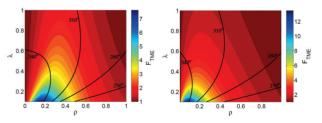

Figure 2: The parametrization of the emittance reduction factor F_{TME} with ρ and λ for the step (left) and the trapezium (right) profile. The black contour lines correspond to different values of the horizontal phase advance.

areas where the reduction is insignificant. For both profiles the highest possible reductions are localized in the limits where $\lambda \to 0.1$. The reductions achieved for the trapezium profile are higher than the ones for the step profile [7]. In the case of non uniform dipoles, even for the TME optics conditions, the horizontal phase advance μ_x always depends on ρ and λ. It is clear that remarkable reductions are reached for phase advances lower than the unique phase advance of the uniform dipole's TME ($\mu_x = 284.5°$). This

is important because lower phase advances correspond to smaller chromaticities that is one of the main goals for the optimisation of low emittance cells.

The total bending angles for the step θ_{st} and the trapezium profile θ_{tr} are:

$$\theta_{st} = \frac{L(\lambda + \rho)}{\rho_1(1 + \lambda)}, \ \theta_{tr} = \frac{L(\lambda(-1 + \rho) + \rho \ln \rho)}{\rho_1(-1 + \rho)(1 + \lambda)} \quad (1)$$

If the dipole's bending angles (i.e. the total number of dipoles N_d), length L and minimum bending radius ρ_1 (i.e. maximum bending field) are fixed, these equation show that there is a dependency between λ and ρ. This constraints even further the problem for finding the appropriate ρ (or λ) for reaching a large reduction factor F_{TME}. Varying the bending angle, while keeping L and ρ_1 fixed, changes also the relation between λ and ρ and so the F_{TME}. As shown in Fig. 3, when reducing the number of dipoles, the reduction factor takes in general smaller values for both step and trapezium profiles. On the other hand, the dependence of the reduction factor F_{TME} with the length ratio λ becomes smoother. In that way, a wider range of λ values gives similar emittance reductions, providing thus more flexibility in choosing the characteristics of the bends.
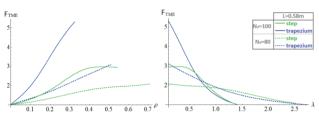

Figure 3: The emittance reduction factor F_{TME} as a function of ρ (left) and λ (right). The solid lines are for $N_d = 100$ and the dashed ones for $N_d = 80$, for the step (green) and trapezium (blue) profiles.

ARC CELL OPTIMIZATION

The variable bends allow the reduction of the number of dipoles (i.e. total number of TME cells) from the existing arc, while the required emittance is still achieved, thereby resulting in a shorter ring (Fig. 3). A pair of (λ, ρ) that gives large reduction factors for $N_d < 100$ is chosen. The dipole length is set to be the same as the one of the present design ($L = 0.58$ m) and the maximum dipole field is set to be 1.77 T for a normal conducting magnet. As soon as the dipoles' characteristics are fixed, the free parameters left for optimizing the TME cell are the drift space lengths. Aiming to solutions with low chromaticities and small quadrupole strengths while keeping the cell compact, several iterations for different drift space lengths and N_d were performed [10]. The optimal solutions are found to be $N_d = 96$ and $N_d = 90$ for the step and the trapezium respectively.

FODO CELL OPTIMIZATION

The damping wigglers are necessary for achieving the low emittance within a fast damping time. Each FODO

structure of the LSS accommodates two wigglers. The use of super-conducting technology is mandatory in order to have a high wiggler field and a relatively short period for obtaining low emittances and fast damping time. It was shown that targeting higher wiggler fields not only the emittance but also the IBS effect can be reduced [11]. The plots in Fig. 4 show the parametrization of the steady state emittance and the IBS effect with the wiggler peak field B_w. For both profiles the wiggler field growth corresponds to a decrease of the IBS effect. Based on the results shown in Fig. 4 and
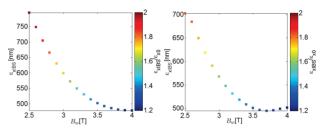

Figure 4: Dependence of the steady state emittance ($\epsilon_{x;IBS}$) and its ratio with the equilibrium one ($\epsilon_{x;IBS}/\epsilon_{x0}$) on the wiggler peak field B_w, for the step (right) and the trapezium (left) profile.

on the technological restrictions, a new working point for the damping wigglers is proposed to be at 3.5 T and with 49 mm period length. This design necessitates a different wire technology using Nb_3Sn material [12]. Under this choice, the FODO cells per LSS can be reduced from 13 down to 10. The final lattices are produced for both profiles. The matched optics of one arc TME cell followed by the dispersion suppressor-beta matching section and one FODO cell are given in Fig. 5 for both profiles. The two rings parameters as compared to the original design are displayed in Table 1. The rings become quite shorter (around 15 % for the step and 20 % for the trapezium variable bends), whereas the damping times are reduced drastically. This is beneficial for all collective effects including IBS. In fact, both lattices reach the target emittances including IBS as calculated by the Bjorken-Mtingwa formalism through MADX [13], whereas the horizontal emittance of the original design is larger [1].
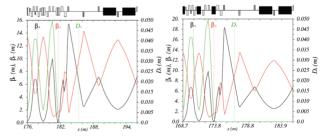

Figure 5: Optical functions of one TME cell, the dispersion suppressor-beta matching section and one FODO cell when using in the arcs the step (left) and the trapezium (right) profile.

---

[1] Using the Piwinski formalism, the original design was also reaching the target horizontal emittance.

Table 1: Design Parameters for the CLIC DRs for the Original and the Improved Designs with Variable Bends

Parameters, Symbol [Unit]	uniform	step	trapezium
Energy, E [GeV]		2.86	
Bunch population, N [10^9]		4.1	
Circumference, C [m]	427.5	374.1	359.4
Basic cell type in the arc/LSS		TME/FODO	
Number of arc cells/wigglers, N_d/N_w	100/52	96/40	90/40
Dipole field (max/min), B_0 [T]	0.97/0.97	1.77/1.01	1.77/0.72
Norm. gradient in dipole [m^{-2}]		-1.1	
Horizontal, vertical tune, (Q_x,Q_y)	(48.35,10.40)	(47.39,9.45)	(44.15,9.23)
Horizontal, vertical chromaticity, (ξ_x,ξ_y)	(-113,-82)	(-135,-76)	(-126,-72)
Wiggler peak field, B_w [T]	2.5	3.5	3.5
Wiggler length, L_w [m]		2	
Wiggler period, λ_w [cm]	5.0	4.9	4.9
Damp. times, (τ_x,τ_y,τ_l) [ms]	(2.0,2.0,1.0)	(1.2,1.3,0.6)	(1.2,1.2,0.6)
Mom. compaction, α_c [10^{-4}]	1.3	1.3	1.2
Energy loss/turn, U [MeV]	4.0	5.7	5.7
Norm. horizontal emit., $\gamma\epsilon_x$ [nm-rad]	681	502	500
Norm. vertical emit., $\gamma\epsilon_y$ [nm-rad]	5.0	4.9	4.9
Energy spread (rms), σ_δ [%]	0.12	0.13	0.13
Bunch length (rms), σ_s [mm]	1.8	1.6	1.6
Long. emittance, ϵ_l [keVm]	5.9	6.1	6.0
IBS factors hor./ver./long.	2.2/1.5/1.2	1.4/1.5/1.1	1.4/1.5/1.1
RF Voltage, V_{RF} [MV]	5.10	7.25	6.97
Stationary phase [^{o}]	51.4	51.3	54.2
Synchrotron tune, Q_s	0.0072	0.0081	0.0075
Harmonic number, h	1425	1248	1199

DYNAMIC APERTURE

The dynamic aperture (DA) of the ring was computed for particles tracked with the PTC module of MADX [13]. Fig. 6 shows the initial positions of particles that survived
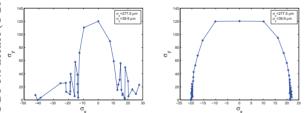

Figure 6: The on momentum dynamic aperture of the DR for the step (right) and the trapezium (left) profile.

over 1000 turns, normalized to the horizontal and vertical beam sizes, at the point of calculation (σ_x = 277.5 μm, σ_y = 39.9 μm). Regarding the fact that the magnets fringe fields are taken into account while the magnet error effects are neglected, the resulted DA seems to be comfortable enough for both profiles. A working point optimisation with simulations including the non-linear effect of wigglers and the space charge tune-shift, including working point optimisation is needed to fully qualify the non-linear performance of the new design.

CONCLUSION

By using TME cells with variable field bends for two different profiles (bending radius following a step and a trapezium shape) and Nb$_3$Sn high-field wigglers (3.5 T), two alternative DR designs are proposed. They achieve all target parameters, for reduced circumferences. The effect of IBS is proved to be well under control and the reduced damping times could certainly be beneficial for all instabilities and feedback system's specifications. As the chromaticities are kept quite low, the new designs proposed here achieve adequate DAs that can be improved after a non-linear optimization and a further working point analysis.

ACKNOWLEDGEMENTS

REFERENCES

[1] Y. Papaphilippou et al., "Conceptual design of the CLIC damping rings", TUPPCO86, proc. of IPAC'12, New Orleans, USA (2012).

[2] Y. Papaphilippou, F. Antoniou, M. Barnes, S. Calatroni, P. Chiggiato, R. Corsini, A. Grudiev, E. Koukovini, T. Lefevre, M. Martini, et al., Tech. Rep. CERN-ATS-2012-176, 2012.

[3] J. Guo and T. Raubenheimer, proc. of EPAC 2002, Paris (2002).

[4] R. Nagaoka, A.F. Wrulich, Nucl. Instrum. Methods Phys. Res., Sect. A 575, 292 (2007).

[5] Y. Papaphilippou, P. Elleaume, PAC 2005, Knoxville (2005).

[6] Y. Papaphilippou, A. Ropert, P. Elleaume, L. Farvacque, proc. of PAC05, Tennessee, USA (2005).

[7] C.-x Wang, Y. Wang, Y. Peng, PRST-AB 14, 034001 (2011).

[8] C.-x Wang, PRST-AB 12, 061001 (2009).

[9] S. Papadopoulou, F. Antoniou and Y. Papaphilippou, Emittance reduction with variable bending magnet strengths: Analytical optics considerations, preprint (2015).

[10] F. Antoniou, Y. Papaphilippou, PRST-AB 17, 064002 (2014).

[11] D. Schoerling et al, PRST-AB 15, 042401 (2012).

[12] L. Garcia Fajardo, "Nb3Sn prototype progress", CLIC Workshop, CERN, Geneva (2015).

[13] MAD-X homepage, http://mad.web.cern.ch/mad.